








# The Voltage-Gated Potassium Channel *Shal* (K<sub>v</sub>4) Contributes to Active Hearing in *Drosophila*

 Eli S. Gregory,<sup>1</sup>  YiFeng Y. J. Xu,<sup>2,3</sup>  Tai-Ting Lee,<sup>2,3</sup>  Mei-ling A. Joiner,<sup>1</sup>  
 Azusa Kamikouchi,<sup>2,3</sup>  Matthew P. Su,<sup>2,3,4</sup> and  Daniel F. Eberl<sup>1</sup>

<sup>1</sup>Department of Biology, University of Iowa, Iowa City, Iowa 52242, <sup>2</sup>Graduate School of Science, Nagoya University, Nagoya 464-8602, Japan, <sup>3</sup>Institute of Transformative Bio-Molecules, Nagoya University, Nagoya 464-8601, Japan, and <sup>4</sup>Institute for Advanced Research, Nagoya University, Nagoya 464-8601, Japan

## Abstract

The full complement of ion channels which influence insect auditory mechanotransduction and the mechanisms by which their influence is exerted remain unclear. *Shal* (K<sub>v</sub>4), a *Shaker* family member encoding voltage-gated potassium channels in *Drosophila melanogaster*, has been shown to localize to dendrites in some neuron types, suggesting the potential role of *Shal* in *Drosophila* hearing, including mechanotransduction. A GFP trap was used to visualize the localization of the *Shal* channel in Johnston's organ neurons responsible for hearing in the antenna. *Shal* protein was localized strongly to the cell body and inner dendritic segment of sensory neurons. It was also detectable in the sensory cilium, suggesting its involvement not only in general auditory function but specifically in mechanotransduction. Electrophysiological recordings to assess neural responses to auditory stimuli in mutant *Shal* flies revealed significant decreases in auditory responses. Laser Doppler vibrometer recordings indicated abnormal antennal free fluctuation frequencies in mutant lines, indicating an effect on active antennal tuning, and thus active transduction mechanisms. This suggests that *Shal* participates in coordinating energy-dependent antennal movements in *Drosophila* that are essential for tuning the antenna to courtship song frequencies.

**Key words:** active hearing mechanism; Kv4; mechanotransduction; sensory cilia; *Shal*; voltage-gated potassium channel

Received Feb. 28, 2024; revised Dec. 3, 2024; accepted Dec. 3, 2024.

The authors declare no competing financial interests.

Author contributions: E.S.G., M.-I.A.J., A.K., M.P.S., and D.F.E. designed research; E.S.G., Y.Y.J.X., T.-T.L., M.-I.A.J., and D.F.E. performed research; E.S.G., Y.Y.J.X., M.-I.A.J., M.P.S., and D.F.E. analyzed data; E.S.G., A.K., M.P.S., and D.F.E. wrote the paper.

We thank Susan Tsunoda for providing flies with the *Shal* dominant-negative construct. Stocks obtained from the Bloomington *Drosophila* Stock Center (NIH P40OD018537) were also used in this study. Monoclonal antibodies were obtained from the Developmental Studies Hybridoma Bank, created by the National Institute of Child Health and Development of the National Institutes of Health and maintained at The University of Iowa, Department of Biology.

Continued on next page.

## Significance Statement

The study of fruit fly hearing has revealed mechanosensitive ion channels that participate in mechanotransduction, and as in mammalian hearing, energy-dependent mechanisms actively amplify and tune auditory processes. Identifying distinct roles played by different ion channels is essential to better understand this process. Here, we explore the influence of a specific voltage-gated potassium channel, *Shal*, on fly hearing and find that it affects specific parts of the mechanotransduction process. Our research uncovers *Shal*'s localization in sensory dendrite regions of auditory neurons, where it contributes to shaping mechanotransduction and active antennal tuning. Understanding *Shal*'s involvement in auditory function and mechanotransduction deepens our knowledge of fly hearing and unveils a key player in the coordination of energy-dependent active antennal movements.

## Introduction

Several ion channels participating in insect auditory mechanosensory transduction have been identified, but the precise transduction mechanisms are still poorly understood. For example, the TRPN channel, encoded by the *no mechanotransduction potential C* (*NompC*; Walker et al., 2000; Göpfert and Robert, 2003; Effertz et al., 2011) gene in

*Drosophila*, and the TRPV channel, comprising two subunits encoded by *inactive* (*lav*) and *nanchung* (*nan*) genes (Kim et al., 2003; Gong et al., 2004; B. Li et al., 2021), are central to mechanotransduction, but their precise contributions are yet to be fully established. These channels localize to the sensory cilia of chordotonal organs, also called scolopidia, which make up Johnston's organ (JO) in the antenna, with NompC localizing distal to the ciliary dilation (Lee et al., 2010) and *lav/Nan* localizing in the ciliary segment proximal to the ciliary dilation (Kim et al., 2003; Gong et al., 2004). Different lines of evidence support two prevailing models of auditory mechanotransduction, known as the NompC model and the *lav/Nan* model (Eberl et al., 2016; Hehlert et al., 2021). In the NompC model, TRPN and TRPV act in series, with the NompC channel functioning as the primary mechanotransduction channel to provide the initial transduction current and *lav/Nan* required for propagation as well as providing additional mechanosensitivity. In contrast, the *lav/Nan* model attributes mechanosensitivity to *lav/Nan*, with NompC acting in parallel to control amplification gain (Albert and Göpfert, 2015; Eberl et al., 2016; Hehlert et al., 2021).

The sensory dendrite, in addition to being the site of the initial transduction event to generate receptor potentials in response to mechanosensory stimulation, is also involved in active mechanisms. By inserting energy into spontaneous movements of the antenna (Göpfert and Robert, 2003; Göpfert et al., 2005), sensory responses to low amplitude stimulation can be amplified, and antennal movements are tuned to enhance reception of sound frequencies related to the *Drosophila* courtship song (Riabinina et al., 2011). These active movements are thought to arise from two sources: first, energy representing reduced mechanical compliance upon transduction channel closing, returning kinetic energy into movement of the antenna (Albert et al., 2007; Nadrowski et al., 2008; Effertz et al., 2012), second, active ciliary movement generated by the ATP-dependent axonemal dynein motors in the proximal segment of the sensory cilium (Eberl, 1999; Karak et al., 2015). It is unclear if and how additional ion channels beyond NompC/*Nan*/*lav* may contribute to the excitability of the sensory cilia in JO, though a number of promising targets exist. This includes the voltage-gated potassium channel encoded by the *Shal* gene, orthologous to  $K_v4$  (Butler et al., 1990; Tsunoda and Salkoff, 1995; Ping et al., 2011), previously shown in other neurons to localize to dendrites rather than axons (Diao et al., 2010) and expressed in JO neurons of adult flies (Fly Cell Atlas; H. Li et al., 2022). If *Shal* indeed localizes in the dendrites, it has the potential to contribute to shaping JO neuron receptor potentials.

Here we first demonstrate that *Shal* is expressed in JO neurons and localizes to the sensory dendrites, including the sensory cilium. Moreover, we show that *Shal* loss-of-function genotypes result in severe reductions in auditory function, as determined by electrophysiology from the antennal nerve. Furthermore, we found using laser Doppler vibrometry (LDV) that these genotypes disrupt the active mechanisms in JO neurons, especially impairing the active tuning to courtship song frequencies. The  $K_v4$  channel encoded by *Shal* thus plays a key role in active transduction mechanisms in insect hearing.

## Materials and Methods

**Fly strains.** *Drosophila melanogaster* genotypes used in this study are listed in Table 1. Controls included the wild-type Canton S strain, as well as *TM3*, *Sb* heterozygotes from the *Shal*<sup>M100446</sup> strain, and, in some experiments, *w elav*<sup>C155</sup>;; *TM6B*, *Tb Hu/+* flies resulting from outcrossing the balanced dominant-negative flies listed in the table with a cantonized *w*<sup>1118</sup> strain. In all experiments, the different controls were tested to ensure no significant differences before pooling. For all experiments, *Shal*<sup>M100446</sup> flies were homozygotes selected from the balanced stock, and dominant-negative *Shal* flies were of the genotype shown in the table. For each experiment, both male and female flies were used, with sex noted in primary data, though no differences were seen between sexes.

**Antibody staining and imaging.** *Drosophila* pupal heads were dissected in cold phosphate-buffered saline (PBS) and then fixed in 4% paraformaldehyde for 15 min. After three washes in PBS with 0.2% Tween-20 (PBT) with rotation over 30 min, the samples were blocked with blocking buffer (BB; freshwater fish skin gelatin, normal goat serum, and bovine serum albumin in PBT) for 1 h with rotation. Primary antibodies diluted in BB included mouse anti-FLAG antibody (1:100; Sigma-Aldrich; RRID:AB\_796202), mouse anti-GFP antibody (1:500; Thermo Fisher Scientific; RRID:AB\_2335261), anti-HA

We thank anonymous reviewers for constructive comments and suggestions. Funding is acknowledged from National Science Foundation Grant 2037828 (to Alan Kay, D.F.E., and Zahre Aminzare); Iowa Office for Undergraduate Research (E.S.G.); Japan Society for the Promotion of Science Invitational Fellowships for Research in Japan (short-term; S22091 to D.F.E.); Nagoya University Neuroscience Institute (D.F.E.); International Principal Investigator (PI) Invitation Program, Nagoya University (D.F.E.); Japan Science and Technology Agency Fusion Oriented Research for disruptive Science and Technology (JPMJFR2147 to A.K.); and Tokai Pathways to Global Excellence, Nagoya University (0121an0002 to M.P.S.).

Correspondence should be addressed to Daniel F. Eberl at daniel-eberl@uiowa.edu.

Copyright © 2025 Gregory et al. This is an open-access article distributed under the terms of the Creative Commons Attribution 4.0 International license, which permits unrestricted use, distribution and reproduction in any medium provided that the original work is properly attributed.

**Table 1. *Drosophila* genotypes used in this study**

Line	Research resource identifier	References
Canton S (Hotta)		
$w^{1118}; PBac\{WH\}Shal^{f00495}$	RRID: BDSC_18338	(Thibault et al., 2004)
$w^{1118}; Mi\{ET1\}Shal^{MB05249}$	RRID: BDSC_24326	(Metaxakis et al., 2005; Bellen et al., 2011)
$y^1 w^*; Mi\{MIC\}Shal^{MI00446}/TM3, Sb$	RRID: BDSC_31006	(Venken et al., 2011)
$y^1 w^*; Mi\{MIC\}Shal^{MI10881}$	RRID: BDSC_56089	(Venken et al., 2011)
$y^1 w^*; Mi\{PT-GFSTF.1\}Shal^{MI00446-GFSTF.1}$	RRID: BDSC_60149	(Nagarkar-Jaiswal et al., 2015)
$w\ elav^{C155-Gal4}; UAS-HA-Shal^{W362F}/TM6B, Tb Hu$		(Ping et al., 2011)

rMs-IgG1 (1:500; Developmental Studies Hybridoma Bank; RRID:AB\_3105930), and rabbit anti-HRP antibody (1:500; Cappel). Primary antibody incubation took place overnight at 4°C with rotation.

The following day, the samples were washed three times in PBT over 30 min with rotation and then incubated with secondary antibodies and phalloidin for 2 h at room temperature with rotation. Secondary antibody diluted in BB (1:500) consisted of goat anti-mouse Oregon Green (488; Thermo Fisher Scientific; RRID:AB\_2539797) and goat anti-rabbit TRITC (Jackson Immunoresearch Laboratories; RRID:AB\_261740), along with phalloidin 405 (1:1,000; Thermo Fisher Scientific). Samples underwent two 15 min washes in PBT with rotation followed by a brief 5 min wash in PBS. Finally, samples were mounted in Fluoromount (Thermo Fisher Scientific; RRID:SCR\_015961) onto glass slides with 1.5 coverslips and imaged with a Leica STELLARIS 8 confocal microscope, using a 63× objective lens with oil immersion. Images were adjusted by applying brightness and contrast changes uniformly to the entire image in each channel using the Fiji software (RRID: SCR\_002285).

**Electrophysiology.** Sound-evoked potentials (SEPs) were captured using a pair of electrolytically sharpened tungsten recording electrodes (Eberl et al., 2000; Eberl and Kernan, 2011). The recording electrode was inserted between the first and second segments of the antennae, while the reference electrode was inserted into the head cuticle near the posterior orbital bristle. A computer-generated pulse song was introduced frontally to the fly under near-field conditions.

Signals were subtracted and amplified with a differential amplifier (DAM50, World Precision Instruments) and digitized at 10 kHz (USB-6001, National Instruments). Average response values were measured as the max–min values in an averaged trace from 10 consecutive presentations of the described protocol.

**LDV data collection.** Following 2 d of entrainment in a 12:12 LD regime, male and female *Drosophila* aged between 3 and 10 d old were aspirated into micropipette tips as for electrophysiology experiments. Fly head movement was restricted by the application of modeling clay to the edge of the pipette. Blue light-cured glue was then applied to the entirety of the right antennae (to completely inhibit movement) as well as the base of the left antennae.

The tip with the immobilized fly was then attached to a rod held in a micromanipulator on a vibration isolation table in a temperature-controlled room (set to 25 ± 1°C). The fly was positioned such that its left arista was perpendicular to the beam of a laser Doppler vibrometer (VibroFlex, Polytec).

Unstimulated arista vibrations [denoted as “free fluctuations” (FF)] were first recorded while the fly was awake. The fly was then sedated via continuous CO<sub>2</sub> exposure for 2 min, before another free fluctuation recording was made. These recordings allowed for investigating both active (awake) and passive (sedated) hearing states.

**LDV data analysis: mechanical tuning calculation.** Fast Fourier transforms of recording values were made using the VibSoft Polytec software for frequencies from 1 to 10 kHz. Frequency values below 100 Hz were excluded from analyses due to significant noise in the recordings.

A forced damped oscillator function was applied to transformed data via the lme4 package (version 1.1-33) in R (version 4.3.0) as follows:

$$\dot{X}(\omega) = \frac{\omega \cdot \frac{F_0}{m}}{\sqrt{\left( (\omega_0^2 - \omega^2)^2 + \left( \omega \cdot \frac{\omega_0}{Q} \right)^2 \right)}}$$

where  $F_0$  is the external force strength,  $m$  is the flagellar apparent mass,  $\omega$  is the angular frequency,  $\omega_0$  is the natural angular frequency, and  $Q$  is the quality factor,  $m\omega_0/\gamma$  ( $\gamma$ , damping constant).

This equation used by Göpfert et al. (2005), here derived for  $\dot{X}(\omega)$ , allowed for estimation of the natural angular frequency of recordings from both active and passive states for each fly, enabling calculation of the mechanical tuning frequency,  $f_0$  ( $\omega_0/2\pi$ ).

**LDV data analysis: power gain calculation.** Following Göpfert et al. (2005), power gain calculations utilized the results of the forced damped oscillator function fits by enabling the calculation of the ratio of total fluctuation power of an individual's active and passive states.

We defined power gain as follows:

$$\text{Power gain} = \frac{\omega_a^2 \langle x_a^2 \rangle}{\omega_p^2 \langle x_p^2 \rangle} - 1,$$

where  $\omega_a$  is the natural angular frequency of active system,  $\omega_p$  is the natural angular frequency of passive system,  $\langle x_a^2 \rangle$  is the sum of squared Fourier displacement amplitudes in active state, and  $\langle x_p^2 \rangle$  is the sum of squared Fourier displacement amplitudes in passive state.

After fitting the above damped harmonic oscillator function to raw velocity data and extracting fit parameters, these parameters were used to calculate velocity estimates for the curve fit between 1 and 10,000 Hz. These velocity values were then converted to displacement values using the formula  $X(\omega) = \dot{X}(\omega)/\omega$  and then squared. These squared displacement values were then used to calculate the sums of squared Fourier displacement amplitudes per individual fly.

Natural angular frequency values were calculated from the function fits, while sums of squared Fourier displacement amplitudes were estimated from the following:

$$\langle x_i^2 \rangle = \int_0^\infty x_i^2(\omega) d\omega.$$

**Statistical analysis.** To evaluate statistical differences in mutant SEP data compared with controls, we pooled three control genotypes (see above, Fly strains) after testing for statistical differences by ANOVA. Analysis of mutant genotypes compared with controls utilized Brown–Forsythe ANOVA, given that the data were largely Gaussian but showed heterogeneity of variances among groups. Dunnett's T3 multiple-comparison post hoc test was then applied to compare each group with every other group, with adjustments for multiple comparisons to control the overall Type 1 error rate. For LDV data, Arista Best Frequencies for both awake and sedated conditions were analyzed in the same way as the SEP data. However, power gain and Q were analyzed using Kruskal–Wallis ANOVA, a nonparametric alternative, because the data were significantly non-Gaussian. This was followed by Dunn's multiple-comparison post hoc test to determine specific differences between each experimental group and the pooled control. All statistical analysis and graphing used GraphPad Prism version 9.5.1 (GraphPad Software). In addition, estimation statistics (<https://www.estimationstats.com/>) were conducted for all measures comparing mutant genotypes to controls with data summarized in Table 2.

## Results

### Shal is expressed in JO neurons and localizes to somata and dendrites

In *Drosophila* single-cell RNAseq data, *Shal* is expressed broadly in JO neurons at the adult stage (H. Li et al., 2022; Extended Data Fig. 1–1). A tagged form of *Shal*, when expressed in olfactory projection neurons, has been shown to localize to the soma and dendrites, but not to axons (Diao et al., 2010). Furthermore,  $K_v4.2$  in the rat hippocampus has also been found to localize to dendrites (Sheng et al., 1992). Thus, we tested whether *Shal* channels in JO neurons are localized in the sensory dendrites, where they could contribute to active mechanosensation.

We first used a *Shal* protein trap line, *Shal*<sup>M100446-GFSTF.1</sup>, in which GFP and other tags are fused in-frame with the *Shal* coding sequence in the endogenous locus (Nagarkar-Jaiswal et al., 2015). We found staining for this tagged *Shal* protein in JO neurons. While staining is strongest in the membrane of JO neuron somata, *Shal* staining was also detected at lower intensity in the cilium (Fig. 1A), as indicated relative to the anti-HRP marker which labels neurons, especially the dendrites.

To confirm this localization, we also used an HA-tagged dominant–negative construct (Table 1; Ping et al., 2011) expressed in all neurons with the *elav*<sup>C155</sup>-*Gal4* driver. Anti-HA also showed staining in this genotype in the dendrites colinear with the anti-HRP marker (Fig. 1B). Thus, the expression pattern of *Shal* suggests a physiological role in JO neurons, and its localization to the sensory cilium is consistent with a possible role in sensory transduction mechanisms.

### Shal is required for proper auditory function in *Drosophila*

To test whether auditory function was impaired following *Shal* mutation, we tested several *Shal* loss-of-function genotypes (Table 1, Extended Data Fig. 2–1) for changes in SEPs (Eberl et al., 2000; Eberl and Kernan, 2011). In this electrophysiological assay, field potentials recorded from the antennal nerve at the joint between segments 1 and 2 represent the combined auditory signals in the axons from all JO neurons (Fig. 2A).

In contrast to controls, *Shal* insertion mutants all showed significantly reduced SEP amplitudes (Fig. 2B,C; Brown–Forsythe ANOVA;  $p < 0.0001$ ; Table 2). Compared with controls, two insertion alleles, *Shal*<sup>M100446</sup> and *Shal*<sup>f00495</sup>, showed

**Table 2. Estimation statistics**

Genotype	N	Mean	SD	Mean difference from control	95% confidence intervals of difference
<b>SEPs (Fig. 2C)</b>					
Control	56	913.9	126.8		
<i>Shal</i> <sup>MI00446-GFSTF.1</sup>	9	974.4	72.7	60.6	13.3–126
<i>Shal</i> <sup>MI00446</sup>	9	332.4	45.7	−581	−630 to −543
<i>Shal</i> <sup>f00495</sup>	8	241.1	31.8	−673	−715 to −638
<i>Shal</i> <sup>DN</sup>	10	299.6	61.3	−614	−668 to −570
<i>Shal</i> <sup>MI10881</sup>	8	425.8	36.9	−488	−534 to −453
<i>Shal</i> <sup>MB05249</sup>	10	390.2	38.0	−524	−566 to −487
<b>Arista best freq. (awake; Fig. 3B)</b>					
Control	25	240.9	45.5		
<i>Shal</i> <sup>MI00446-GFSTF.1</sup>	10	273.3	61.5	32.4	2.2–88
<i>Shal</i> <sup>MI00446</sup>	17	340.9	36.1	100	74.0–123
<i>Shal</i> <sup>f00495</sup>	11	423.7	52.5	183	151–219
<i>Shal</i> <sup>DN</sup>	11	338.9	78.2	98.1	57.4–150
<i>Shal</i> <sup>MI10881</sup>	10	197.0	78.2	−43.9	−83.5 to 18.4
<i>Shal</i> <sup>MB05249</sup>	10	260.6	88.0	19.7	−21.5 to 98.2
<b>Arista best freq. (sedated; Fig. 3B)</b>					
Control	25	797.9	94.0		
<i>Shal</i> <sup>MI00446-GFSTF.1</sup>	10	827.5	83.6	29.6	−22.2 to 106
<i>Shal</i> <sup>MI00446</sup>	17	873.1	68.1	75.2	25.9–122
<i>Shal</i> <sup>f00495</sup>	11	758.0	84.2	−39.9	−90.4 to 26.6
<i>Shal</i> <sup>DN</sup>	11	737.7	29.0	−60.1	−99.5 to −21.1
<i>Shal</i> <sup>MI10881</sup>	10	856.0	155	58.1	−36.9 to 161
<i>Shal</i> <sup>MB05249</sup>	10	796.3	80.9	−1.5	−60 to 56.6
<b>Power gain (Fig. 3C)</b>					
Control	25	7.32	7.9		
<i>Shal</i> <sup>MI00446-GFSTF.1</sup>	10	13.6	20.3	6.3	−1.7 to 28
<i>Shal</i> <sup>MI00446</sup>	17	20.1	25.0	12.8	3.7–30
<i>Shal</i> <sup>f00495</sup>	11	2.61	2.8	−4.7	−8.6 to −1.6
<i>Shal</i> <sup>DN</sup>	11	2.82	2.1	−4.9	−8.5 to −1.6
<i>Shal</i> <sup>MI10881</sup>	10	6.43	4.8	−0.9	−5.2 to 3.1
<i>Shal</i> <sup>MB05249</sup>	10	2.60	4.1	−4.7	−8.4 to −0.7
<b>Q (awake; Extended Data Fig. 3-1A)</b>					
Control	25	1.20	0.43		
<i>Shal</i> <sup>MI00446-GFSTF.1</sup>	10	1.80	0.46	0.60	0.31–0.96
<i>Shal</i> <sup>MI00446</sup>	17	2.66	1.74	1.46	0.83–2.54
<i>Shal</i> <sup>f00495</sup>	11	0.68	0.17	−0.52	−0.75 to −0.36
<i>Shal</i> <sup>DN</sup>	11	0.43	0.13	−0.77	−1.00 to −0.62
<i>Shal</i> <sup>MI10881</sup>	10	1.47	2.02	0.28	−0.45 to 2.39
<i>Shal</i> <sup>MB05249</sup>	10	1.26	0.64	0.06	−0.25 to 0.62
<b>Q (sedated; Extended Data Fig. 3-1B)</b>					
Control	25	0.96	0.20		
<i>Shal</i> <sup>MI00446-GFSTF.1</sup>	10	0.94	0.23	−0.02	−0.15 to 0.15
<i>Shal</i> <sup>MI00446</sup>	17	1.02	0.26	0.06	−0.07 to 0.19
<i>Shal</i> <sup>f00495</sup>	11	1.00	0.17	0.04	−0.08 to 0.14
<i>Shal</i> <sup>DN</sup>	11	1.01	0.18	0.05	−0.11 to 0.15
<i>Shal</i> <sup>MI10881</sup>	10	1.04	0.21	0.08	−0.05 to 0.23
<i>Shal</i> <sup>MB05249</sup>	10	1.11	0.20	0.15	−0.01 to 0.26

the most reduced SEPs (Fig. 2C; Dunnett's T3 multiple comparisons;  $p < 0.0001$  each; Extended Data Fig. 2-1; Table 2), while *Shal*<sup>MI10881</sup> and *Shal*<sup>MB05249</sup> showed SEPs that were significantly reduced compared with controls (Dunnett's;  $p < 0.0001$  each; Table 2) but significantly higher than the other two alleles (Fig. 2B,C; Dunnett's;  $p$  values between 0.006 and  $< 0.0001$ ; Extended Data Fig. 2-1). To test for possible changes in hearing function, we also tested the protein trap line *Shal*<sup>MI00446-GFSTF.1</sup>, derived from *Shal*<sup>MI00446</sup> by replacing the MiMIC cassette in the insertion with the GFSTF marker cassette flanked by splice acceptor and splice donor sites (Table 1, Extended Data Fig. 2-1) to generate full-length *Shal* proteins with the markers fused in-frame (Nagarkar-Jaiswal et al., 2015). SEPs of this protein trap line were not significantly different from controls (Dunnett's;  $p = 0.60$ ; Table 2) but significantly different from the parent *Shal*<sup>MI00446</sup> allele (Fig. 2C; Dunnett's;  $p < 0.0001$ ), suggesting that the fusion protein is fully functional for this phenotype.

Finally, flies expressing the *Shal* dominant-negative construct in all neurons also showed strong reduction in SEPs compared with controls, (Fig. 2C; Dunnett's;  $p < 0.0001$ ; Table 2). *Shal* dominant-negative SEPs were not significantly different

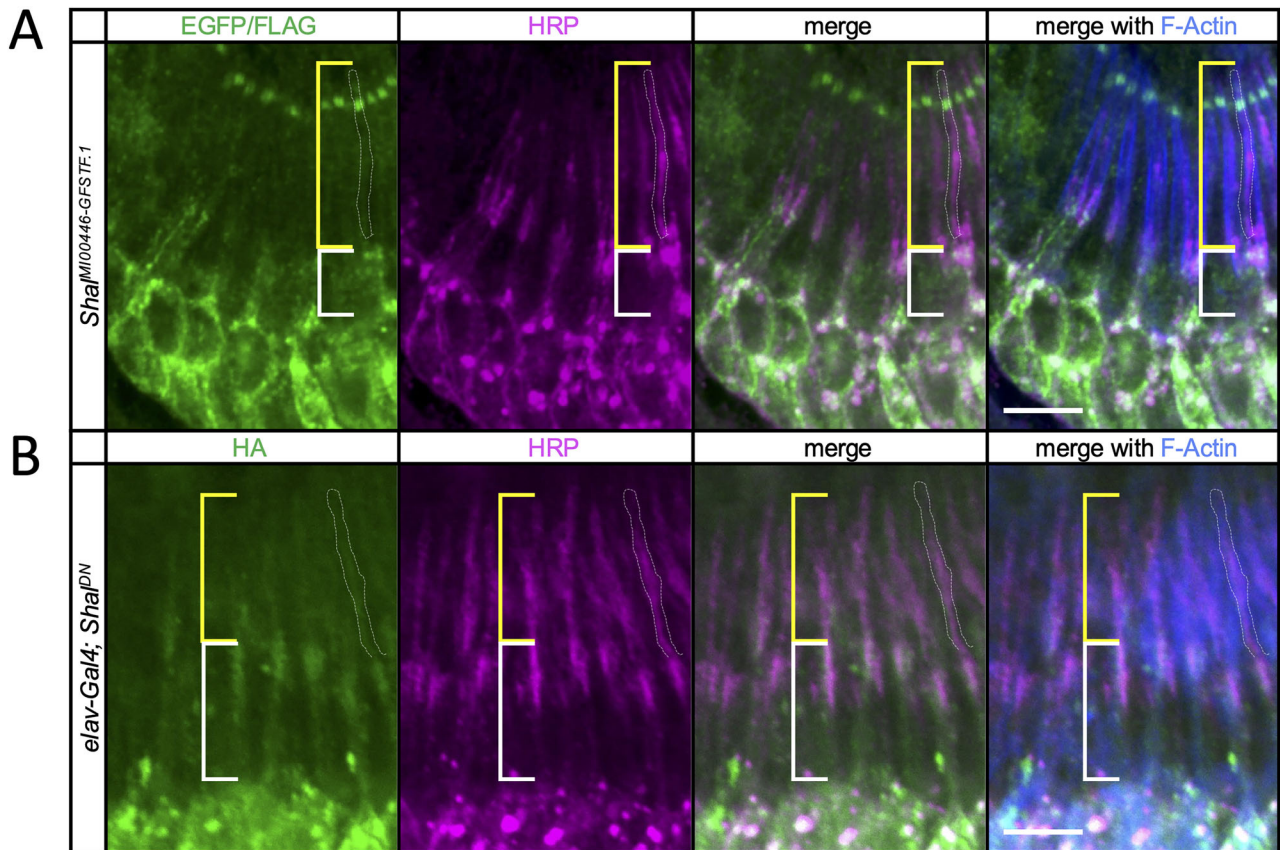


**Figure 1.** Shal is expressed in JO neurons and localizes to sensory dendrites and somata. **A**, Immunostaining of pupal JO from the Shal protein trap line, *Shal*<sup>M100446-GFSTF.1</sup>. The tagged Shal protein is stained with anti-EGFP and anti-FLAG in the green channel. Neurons are visualized with anti-HRP (magenta) which shows enhanced dendrite staining. Phalloidin (blue) stains the scolopale rods in the scolopale cell surrounding the sensory dendrite. Brackets indicate the inner (white bracket) and outer (yellow bracket) dendritic segments. White-dotted outline indicates an example cilium. Scale bar, 5  $\mu$ m. **B**, Immunostaining of pupal JO from flies expressing the Shal dominant-negative construct, *UAS-HA-Shal*<sup>W362F</sup>, in neurons. Anti-HA staining shows the dominant-negative construct in green, with anti-HRP (magenta) and phalloidin (blue). Brackets and white-dotted outline as in **A**. Scale bar, 5  $\mu$ m. For expression of Shal in the Fly Cell Atlas antennal single nucleus RNA sequencing data, see Extended Data Figure 1-1.

from the stronger insertion alleles, *Shal*<sup>M100446</sup> and *Shal*<sup>I00495</sup> (Fig. 2C; Dunnett's;  $p = 0.97$  and  $p = 0.28$ , respectively) but significantly more reduced than the two weaker insertion alleles, *Shal*<sup>M10881</sup> and *Shal*<sup>MB05249</sup> (Fig. 2C; Dunnett's;  $p = 0.0014$  and  $p = 0.022$ , respectively).

In summary, all mutant or dominant-negative genotypes resulted in significant SEP reductions, and the protein trap fusion restored function to the mutant insertion from which it was derived. Taken together, this indicates that *Shal* plays critical roles in sending auditory signals to the brain.

### Shal is required for tuning antennal active movements

To test whether Shal channel activity in the ciliated dendrite is important for active mechanosensation to tune the antenna's resonant frequency as well as energy injection into antennal movement, we measured FF of *Shal* mutant and control fly antennae, both awake and under CO<sub>2</sub> sedation, using LDV (Göpfert and Robert, 2003; Göpfert et al., 2005; Weinberger et al., 2017; Fig. 3A). By fitting a previously published damped harmonic oscillator fit to this LDV data, we were able to estimate key parameters. In awake flies, we found significant differences in resonant frequency based on genotype (Fig. 3B; Brown-Forsythe ANOVA;  $p < 0.0001$ ; Table 2). The antennal resonant frequency of awake control flies was  $240.9 \pm 9.1$  Hz (mean  $\pm$  SEM; Fig. 3B). Among *Shal* insertion mutants, *Shal*<sup>MB05249</sup> and *Shal*<sup>M10881</sup> flies showed no significant change in awake tuning, with  $260.6 \pm 27.8$  and  $197.0 \pm 24.7$  Hz, respectively (Fig. 3B; Dunnett's T3 multiple comparisons;  $p > 0.9999$  and  $p = 0.84$ , respectively; Table 2). In contrast, *Shal*<sup>I00495</sup> and *Shal*<sup>M100446</sup> flies showed significant increases in awake tuning, with  $423.7 \pm 15.8$  and  $340.9 \pm 8.8$  Hz, respectively (Fig. 3B; Dunnett's;  $p < 0.0001$  each; Table 2). Furthermore, the dominant-negative *Shal* flies also showed increased awake tuning of  $338.9 \pm 23.6$  Hz (Fig. 3B; Dunnett's;  $p < 0.033$ ; Table 2). Meanwhile, the *Shal* protein trap flies were not distinguishable from controls, at  $273.3 \pm 19.4$  Hz (Dunnett's;  $p = 0.091$ ; Table 2).

Sedation with CO<sub>2</sub> removes physiologically active processes, leaving only passive mechanical movements of the antenna (Fig. 3A; Göpfert and Robert, 2003; Göpfert et al., 2005; Weinberger et al., 2017). Under sedation, we found the resonant

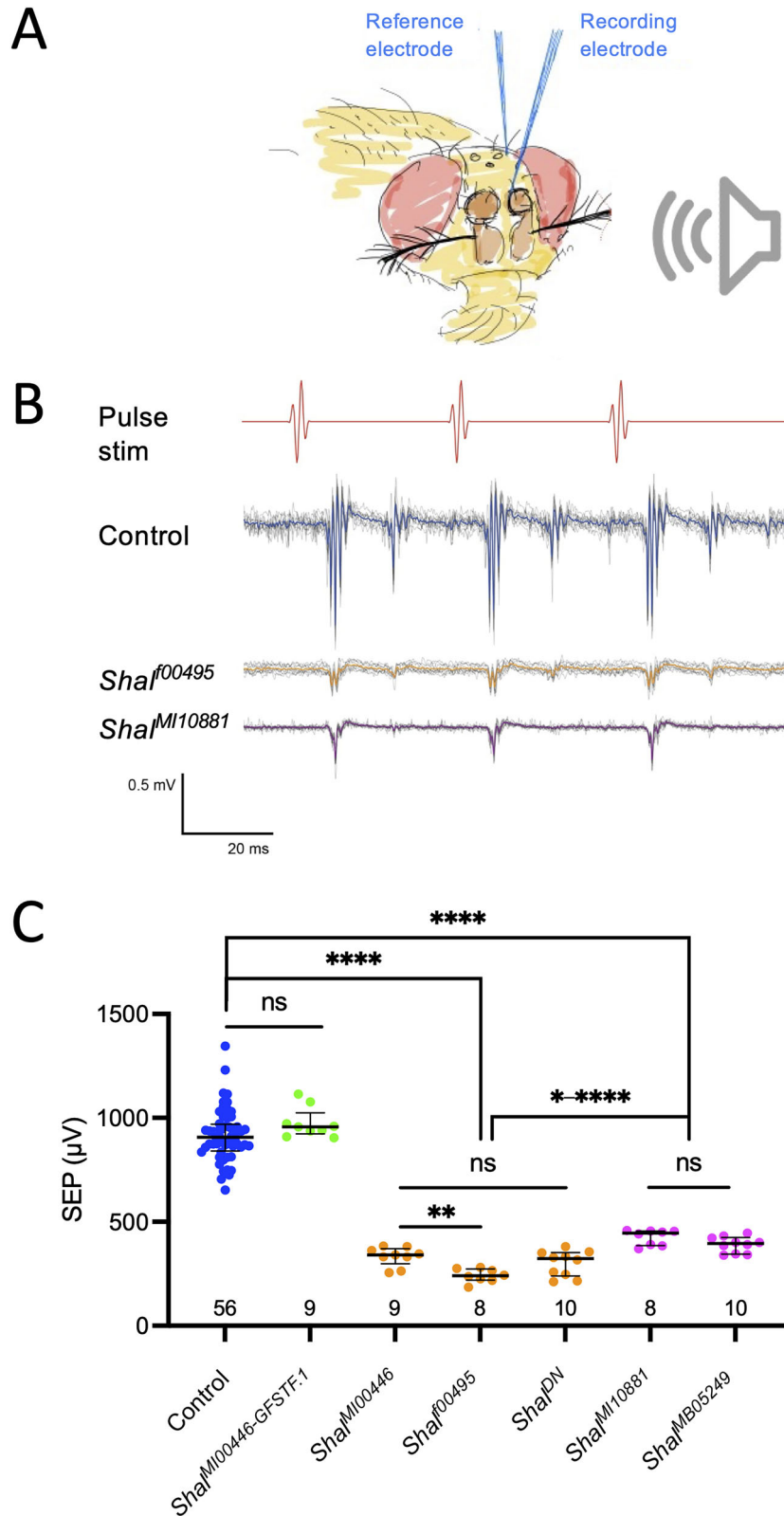


**Figure 2.** *Shal* loss of function impairs auditory signals in the antennal nerve. **A**, Schematic of electrophysiological recording preparation. SEPs are recorded as differential field potentials from a tungsten electrode placed near the antennal nerve (recording electrode) relative to one inserted in the dorsal head capsule (reference electrode) in response to presentation of near-field acoustic stimuli. **B**, Example traces from control and mutant flies in response to synthetic pulse song stimulus. Individual responses to 10 consecutive stimuli are depicted as thin gray lines and their average as the thicker blue (control), orange (mutant), or magenta (mutant) line, in agreement with the color scheme in **C**. **C**, Scatterplot of SEP amplitudes recorded from flies with *Shal*-related genotypes. Smaller delayed responses represent acoustic echo artifacts. Each dot represents the SEP amplitude recorded from one antenna, and the

frequency of control flies to be  $797.9 \pm 18.8$  Hz (Fig. 3B), as expected from previous reports (Riabinina et al., 2011). We also found all *Shal* genotypes tested to show passive resonant frequencies in the same range (Fig. 3B) and not significantly different from controls (Dunnett's multiple-comparison  $p$  values ranging from  $p = 0.087$  to  $p > 0.9999$ ; Table 2), although the overall Brown–Forsythe ANOVA was significant at  $p = 0.0058$ , primarily attributable to a difference between *Shal*<sup>M100446</sup> and the *Shal* dominant-negative flies. These findings show that *Shal* has minimal impact on passive mechanical properties of the antenna but is required to shift the antennal tuning from the passive 800 Hz range to the fully active 240 Hz range. Without *Shal* activity in the strongest loss-of-function genotypes, the active tuning shifts only partially, to the 400 Hz range.

Another aspect of tuning is the sharpness of the tuning peak, which can be quantified by estimating the  $Q$  factor from the damped harmonic oscillator fit. When we calculated  $Q$  values in the FF recordings from Figure 3B in awake flies (Extended Data Fig. 3-1A), we found significant differences between control flies and the three genotypes that showed the strongest SEP phenotypes. These differences were not all in the same direction, however, with one line showing an increased tuning sharpness and the others showing decreased tuning sharpness. For sedated flies, we found no differences in  $Q$  factor between all groups (Extended Data Fig. 3-1B; Table 2).

From the active and passive LDV recordings, it is possible to calculate auditory power gain, the active injection of energy into the hearing system representing one measure of the energy provided by the active system above the passive baseline. While a Kruskal–Wallis ANOVA test of power gain calculations (Fig. 3C) shows significant differences by genotype ( $p = 0.0015$ ), none of the individual genotypes is significantly different from controls (Fig. 3C; Dunn's multiple-comparison  $p$  values range from  $p = 0.73$  to  $p > 0.9999$ ; Table 2). Significance in the overall model arises primarily from *Shal*<sup>M100446</sup> versus *Shal*<sup>I00495</sup> (Dunn's  $p = 0.02$ ) and *Shal*<sup>M100446</sup> versus *Shal*<sup>MB05249</sup> (Dunn's  $p = 0.011$ ). Compared with controls, we see no obvious changes in power gain among *Shal* loss-of-function genotypes, suggesting that *Shal* has little effect on the overall energy that JO neurons generate for active mechanosensation.

## Discussion

We have shown that *Shal* is expressed in JO neurons where it is important for the neuronal output, as measured by the electrophysiological signals sent to the brain along the antennal nerve. *Shal* localizes not only to the JO neuron cell bodies but also to the sensory dendrite where it is positioned to participate in active hearing mechanisms. Indeed, our LDV data confirm that loss of *Shal* significantly affects the active physiological tuning of antennal oscillation in the absence of sound. In wild-type flies, such tuning mechanisms shift antennal oscillations from a resonant frequency in the 800 Hz range to the 240 Hz range.

We were surprised to find that some alleles, specifically *Shal*<sup>M110881</sup> and *Shal*<sup>MB05249</sup>, reduced SEPs but had little effect on the active mechanisms of antennal movement. This suggests that *Shal* may have distinct contributions to these active mechanisms, presumably acting in the dendrite, compared with the generation or propagation of the action potential measured in the nerve, functions that may depend more on *Shal* channels localized in the soma. Thus, these two alleles may differ in the specific properties of the *Shal* channel required for localization to these two compartments or of the *Shal* channel  $K^+$  currents as they contribute to these different functions. Alternatively, these two functions may simply differ in their susceptibility to reduced expression levels. Interestingly, the *Shal*<sup>M110881</sup> and *Shal*<sup>MB05249</sup> alleles are inserted into the first intron, in the 5'-UTR region, while the other insertion alleles are inserted in the second intron, located in the coding region (Extended Data Fig. 2-1). This difference in the insertion site may allow any read-through transcripts still to generate normal full-length *Shal* channel proteins for those insertions in the first intron, albeit at reduced levels, while read-through transcripts from those in the second intron will affect the channel structure.

The dominant-negative *Shal* is associated with a single amino acid change, from tryptophan to phenylamine at Position 362 (Ping et al., 2011), located at the pore region, based on a similar mutation in mouse  $K_v4.2$  (Barry et al., 1998).  $K_v4$  channels assemble as tetramers (Kise et al., 2021), and incorporation of  $K_v4.2$ <sup>W362F</sup> subunits has been shown to block channel activity (Barry et al., 1998). Overexpression of *UAS-HA-Shal*<sup>W362F</sup> in the background of normal *Shal* alleles is likely to result in a preponderance of mutant channel subunits, making assembly of a wild-type tetramer rare and leading to a dominant-negative phenotype equivalent to a strong loss-of-function phenotype (Ping et al., 2011). This interpretation is consistent with our results in both the electrophysiological and antennal movement phenotypes (Figs. 2C, 3B). We note that our results with the dominant-negative *Shal* are consistent with our results for insertional loss-of-function alleles for all three phenotypes (localization, electrophysiology, and antenna motion), mitigating concerns of possible off-target effects of the dominant-negative construct. In no case do we make conclusions solely based on the dominant-negative genotype.

←

number of antennae tested for each genotype is indicated at the bottom of the graph. Bars indicate means, and error bars represent SEM. Controls (blue dots) and the *Shal* protein trap flies, *Shal*<sup>M100446-GFSTF.1</sup> (green dots), are not significantly different, but all other genotypes are significantly different from controls. Strong alleles (orange dots) produce significantly lower SEPs than weak alleles (magenta dots). The dominant-negative *Shal* genotype (*Shal*<sup>DN</sup> = *w elav*<sup>C155</sup>-*Gal4*; *UAS-HA-Shal*<sup>W362F</sup>/*TM6B*, *Tb Hu*) behaves as a strong mutant genotype. Brown–Forsythe ANOVA;  $p < 0.0001$ ; with Dunnett's multiple comparisons (ns, not significant; \* $p < 0.05$ ; \*\* $p < 0.01$ ; \*\*\* $p < 0.001$ ; \*\*\*\* $p < 0.0001$ ). For the map of the *Shal* locus and insertional constructs of *Shal* alleles, see Extended Data Figure 2-1.

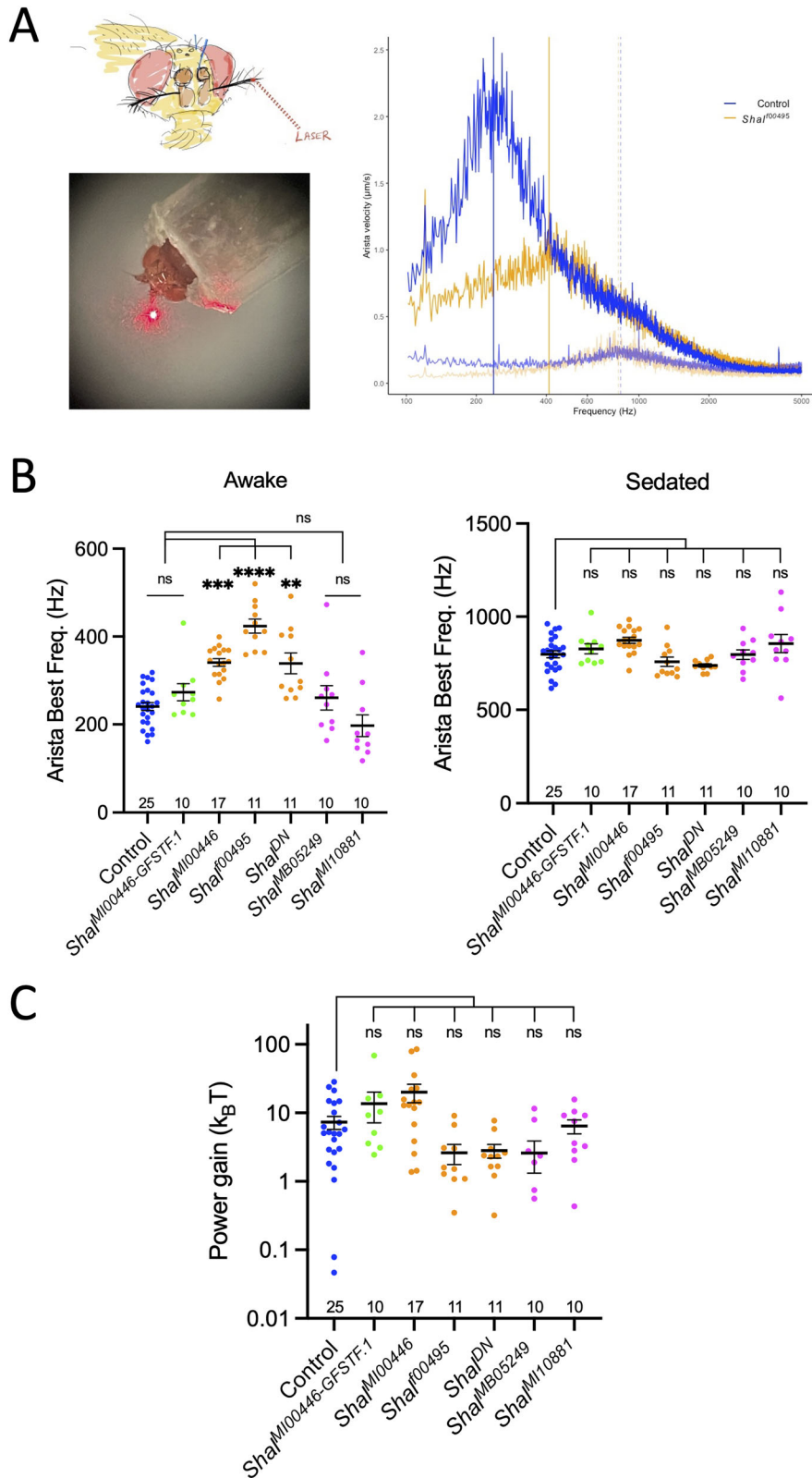


**Figure 3.** *Shal* loss of function shifts antennal resonant frequency with little effect on power gain. **A**, LDV preparation. Reflections from a laser beam focused on the arista allow precise recording of antennal movements. In the awake state, the antenna of a control fly (blue trace) shows vibrations in a range of frequencies below 1.5 kHz, with a peak at ~240 Hz (vertical blue line). The same antenna under CO<sub>2</sub> sedation (light blue trace) shows lower magnitude vibrations with a peak in the 800 Hz range (light blue dashed vertical line). These recordings in the absence of sound stimuli are called “FF.” Similar laser vibrometry recordings from an awake *Shal<sup>f00495</sup>* mutant (orange trace) shows peak vibrations in the 400 Hz range (orange vertical line), but when sedated, vibrations from the same fly (light orange trace) are in the 800 Hz range (light orange dashed vertical line) resembling a sedated control fly. **B**, Scatterplots of

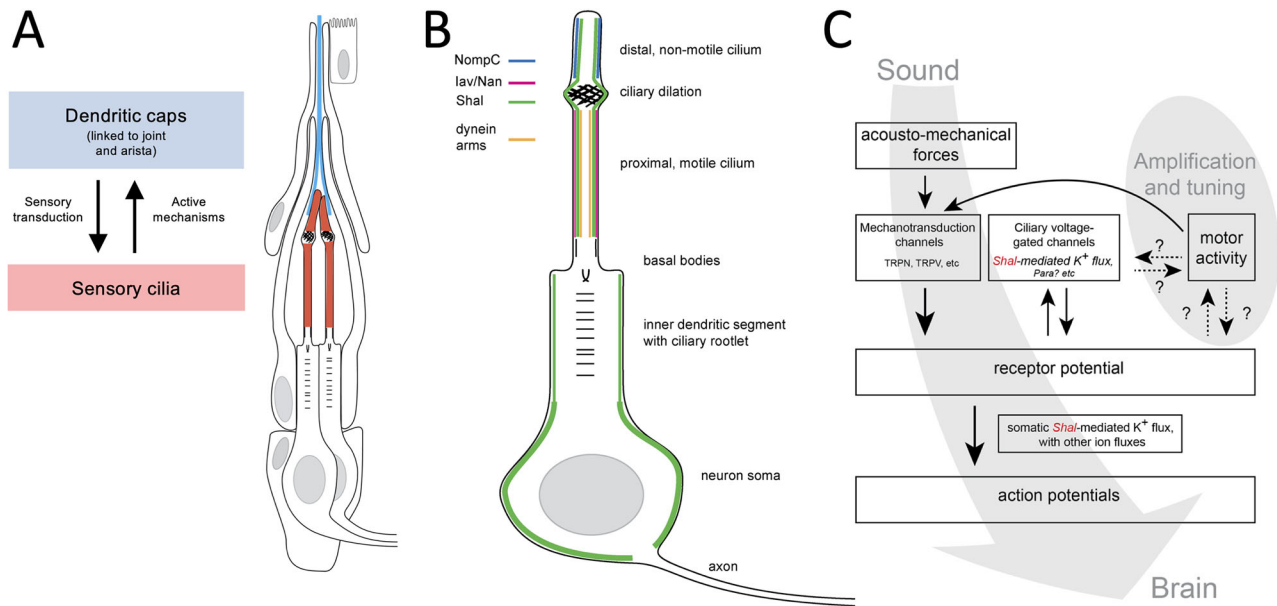


**Figure 4.** Model of Shal in active mechanotransduction in JO. **A**, During sensory transduction, sound-induced movements of the arista are transferred by the dendritic caps (blue) to the JO neuron ciliated dendrites (red) to initiate mechanotransduction. In the absence of sound stimuli, active ciliary movements in the sensory dendrites of JO neurons transfer kinetic energy to the antennal joint via the dendritic cap resulting in antennal vibrations (FF). **B**, In the JO neurons, several ion channels have been localized to the dendritic compartment. NompC (TRPN) is localized in the distal-most ciliary compartment beyond the ciliary dilation. This ciliary segment is nonmotile given the absence of axonemal dynein arms. Nan/lav (TRPV) channels localize in the motile proximal ciliary segment, colinear with the localization of axonemal dynein arms. In this study, we show that Shal localizes at low intensity along the entire sensory cilium and strongly in the neuron soma membrane. **C**, Schematic of complex interplay between the dynamics of membrane currents (receptor potentials) mediated by both TRPN and TRPV and the timing of active ciliary movements. Ciliary localization of Shal is consistent with a role in development of receptor potentials and directly or indirectly affecting motor activity. Alternatively, rather than dynamic cycle-by-cycle gating, we cannot rule out the possibility that Shal provides a static bias in membrane potential that impacts TRPN- and TRPV-mediated currents and active ciliary movements. Either way, loss of Shal may change the receptor potential dynamics sufficiently to shift the motor activity timing, shifting the antennal tuning. Altered tuning together with altered receptor potentials may reduce the activation of action potentials at the axon. Localization of Shal in the inner dendritic segment and in the neuron soma may affect the propagation of the sensory receptor potential or its conversion into an action potential. Some alleles may affect this somatic function, disrupting the generation or propagation of full action potentials without affecting active ciliary movements.

The cellular trafficking mechanisms that localize the Shal protein in JO neuron dendrites are unknown. In olfactory projection neurons, dendritic localization of Shal depends on a di-leucine motif and its interacting protein, Shal-interacting Di-leucine protein (SIDL; Diao et al., 2010). The *Shal* locus has been shown to generate three distinct mRNA splicing isoforms which differ in the 3'-end (Butler et al., 1990; Wei et al., 1990; Extended Data Fig. 2-1). The di-leucine is located at residues 481–482, about seven residues before the divergence of the three isoforms. Thus, all three isoforms contain the di-leucine motif, but as the dendritic targeting was tested in the context of the longest isoform, and it is not known which isoforms are expressed in JO neurons, we cannot be certain whether this dendritic targeting mechanism applies to Shal in JO neurons. Furthermore, while *SIDL* is expressed in JO neurons, its expression level is low (Fly Cell Atlas; H. Li et al., 2022).  $K_v4.2$  and  $K_v4.3$  localization in the rat hippocampus may rely on multiple mechanisms, including localization of the mRNA based on sequences in the 3'-UTR or protein localization through  $K_v$  channel-interacting proteins or membrane-spanning dipeptidyl aminopeptidase-like proteins (Sheng et al., 1992; Nadal et al., 2003; Jo et al., 2010; Alfaro-Ruiz et al., 2019). Whether any of these mechanisms play a role in JO neurons remains to be tested.

The specific mechanism by which dendritic Shal channels shape antennal motion is not known. Active antennal motion is presumably performed by axonemal dyneins (Eberl, 1999; Karak et al., 2015), and their regulation must require appropriate membrane receptor potential dynamics to coordinate the ciliary movement in the correct phase to change the frequency appropriately (Fig. 4). Our findings of minimal effect on power gain in *Shal* mutants (Fig. 3C; Table 2), with effects

the peaks (best frequencies) of antennal FF in the awake state (left graph) and the sedated state (right graph). Each dot represents the best frequency of one antenna, and the number of antennae tested for each genotype is indicated at the bottom of each graph. Bars indicate means; error bars represent SEM. Colors of dots match genotypes of Figure 2. In the awake state, the strong alleles (orange dots) show best frequencies significantly higher than controls (blue dots). However, the weak alleles (magenta dots) as well as the *Shal* protein trap (green dots) do not significantly shift the best frequencies compared with controls. Brown-Forsythe ANOVA;  $p < 0.0001$ ; with Dunnett's multiple comparisons (ns, not significant;  $**p < 0.01$ ;  $***p < 0.001$ ;  $****p < 0.0001$ ). In the sedated state, none of the genotypes significantly differ from controls. Kruskal-Wallis ANOVA with Dunn's multiple comparisons (ns, not significant). For plots of Q values of LDV data for *Shal* genotypes, see Extended Data Figure 3-1.

primarily on tuning, suggest the strength of ciliary activity is largely unaffected but is rather out of phase with membrane potential changes, inhibiting tuning to the desired 240 Hz range. Our estimates of Q values based on free fluctuation fits (Table 2) found no differences in tuning sharpness across genotypes for sedated flies; however, for awake flies, differences were identified. This could indicate the role of membrane voltage in influencing the mechanobiology of ion channels which determine ear stiffness, such as NompC.

One possible mechanism by which Shal channels might affect receptor potential dynamics locally in the dendrite is to sharpen receptor potentials through their fast activation and inactivation kinetics (Butler et al., 1990; Wei et al., 1990; Baldwin et al., 1991; Jerng et al., 2004; Ping et al., 2011). In hippocampal CA1 pyramidal cell dendrites and granule cell dendrites in the dentate gyrus, the transient A-type potassium currents (encoded by  $K_v4$ ) have also been reported to inhibit backpropagation of action potentials, limit the dendritic initiation of action potentials, and dampen the effect of excitatory dendritic inputs (Hoffman et al., 1997; Yang et al., 2015; Oulé et al., 2021). Thus, in JO neuron dendrites, Shal may be shaping the kinetics of one receptor potential as it develops and may also modulate any backpropagation to coordinate with the next cycle of receptor potential activation to sustain active oscillations. Alternatively, we cannot rule out that Shal may bias the membrane currents or receptor potential in a sustained static manner rather than cycle-by-cycle dynamics. Either way, these activities likely also depend on other dendritic ion channels, including NompC and Nan/lav, as well as potentially the voltage-gated sodium channel encoded by the *para* gene, which has also been shown to localize to JO neuron dendrites (Ravenscroft et al., 2023). The interdependence of Shal-mediated  $K^+$  fluxes, axonemal dynein-mediated ciliary motor activity, and receptor potentials are depicted in Figure 4C. However, there remain many open questions. In particular, it will be important to solidify the specific roles of the TRPV and TRPN channels in the development of the receptor potentials. Furthermore, determining the specific ionic composition of the receptor lymph in the scolopale space is important, which, if  $K^+$ -rich as is commonly thought, may affect the rate and perhaps the direction of  $K^+$  flux across the ciliary membrane. Regulation of the dynein arm motor activity, especially the mechanisms by which it coordinates with the membrane electrical activity, must also be resolved. Detailed understanding of how all these channel activities interact to shape receptor potentials and modulate the timing of axonemal dynein arm activity to influence antennal motion will require further investigation.

## References

- Albert JT, Göpfert MC (2015) Hearing in *Drosophila*. *Curr Opin Neurobiol* 34:79–85.
- Albert JT, Nadrowski B, Göpfert MC (2007) Mechanical signatures of transducer gating in the *Drosophila* ear. *Curr Biol* 17:1000–1006.
- Alfaro-Ruiz R, Aguado C, Martín-Belmonte A, Moreno-Martínez AE, Luján R (2019) Expression, cellular and subcellular localisation of  $Kv4.2$  and  $Kv4.3$  channels in the rodent hippocampus. *Int J Mol Sci* 20:246.
- Baldwin TJ, Tsaur M-L, Lopez GA, Jan YN, Jan LY (1991) Characterization of a mammalian cDNA for an inactivating voltage-sensitive  $K^+$  channel. *Neuron* 7:471–483.
- Barry DM, Xu H, Schuessler RB, Nerbonne JM (1998) Functional knockout of the transient outward current, long-QT syndrome, and cardiac remodeling in mice expressing a dominant-negative  $Kv4 \alpha$  subunit. *Circ Res* 83:560–567.
- Bellen HJ, et al. (2011) The *Drosophila* gene disruption project: progress using transposons with distinctive site specificities. *Genetics* 188:731–743.
- Butler A, Wei A, Salkoff L (1990) *Shal*, *Shab*, *Shaw*: three new genes encoding potassium channels in *Drosophila*. *Nucleic Acids Res* 18:2173–2174.
- Diao F, Chaufty J, Waro G, Tsunoda S (2010) SIDL interacts with the dendritic targeting motif of Shal ( $K_v4$ )  $K^+$  channels in *Drosophila*. *Mol Cell Neurosci* 45:75–83.
- Eberl DF (1999) Feeling the vibes: chordotonal mechanisms in insect hearing. *Curr Opin Neurobiol* 9:389–393.
- Eberl DF, Hardy RW, Kernan M (2000) Genetically similar transduction mechanisms for touch and hearing in *Drosophila*. *J Neurosci* 20:5981–5988.
- Eberl DF, Kamikouchi A, Albert JT (2016) Auditory transduction. In: *Insect hearing* (Pollack GS, Mason AC, Popper AN, Fay RR, eds), pp 159–175. Switzerland: Springer International Publishing.
- Eberl DF, Kernan MJ (2011) Recording sound-evoked potentials from the *Drosophila* antennal nerve. *Cold Spring Harb Protoc* 2011: prot5576.
- Effertz T, Nadrowski B, Piepenbrock D, Albert JT, Göpfert MC (2012) Direct gating and mechanical integrity of *Drosophila* auditory transducers require TRPN1. *Nat Neurosci* 15:1198–1200.
- Effertz T, Wiek R, Göpfert MC (2011) NompC TRP channel is essential for *Drosophila* sound receptor function. *Curr Biol* 21:592–597.
- Gong Z, et al. (2004) Two interdependent TRPV channel subunits, inactive and Nanchung, mediate hearing in *Drosophila*. *J Neurosci* 24:9059–9066.
- Göpfert MC, Humphris ADL, Albert JT, Robert D, Hendrich O (2005) Power gain exhibited by motile mechanosensory neurons in *Drosophila* ears. *Proc Natl Acad Sci U S A* 102:325–330.
- Göpfert MC, Robert D (2003) Motion generation by *Drosophila* mechanosensory neurons. *Proc Natl Acad Sci U S A* 100:5514–5519.
- Hehlert P, Zhang W, Göpfert MC (2021) *Drosophila* mechanosensory transduction. *Trends Neurosci* 44:323–335.
- Hoffman DA, Magee JC, Colbert CM, Johnston D (1997)  $K^+$  channel regulation of signal propagation in dendrites of hippocampal pyramidal neurons. *Nature* 387:869–875.
- Jerng HH, Pfaffinger PJ, Covarrubias M (2004) Molecular physiology and modulation of somatodendritic A-type potassium channels. *Mol Cell Neurosci* 27:343–369.
- Jo A, Nam YJ, Oh JY, Cheon HS, Jeromin A, Lee JA, Kim HK (2010) Dendritic localization and a *cis*-acting dendritic targeting element of  $Kv4.2$  mRNA. *BMB Rep* 43:677–682.
- Karak S, Jacobs JS, Kittelmann M, Spalthoff C, Katana R, Sivan-Loukianova E, Schon MA, Kernan MJ, Eberl DF, Göpfert MC (2015) Diverse roles of axonemal dyneins in *Drosophila* auditory neuron function and mechanical amplification in hearing. *Sci Rep* 5:17085.
- Kim J, et al. (2003) A TRPV family ion channel required for hearing in *Drosophila*. *Nature* 424:81–84.
- Kise Y, Kasuya G, Okamoto HH, Yamanouchi D, Kobayashi K, Kusakizako T, Nishizawa T, Nakajo K, Nureki O (2021) Structural basis of gating modulation of  $Kv4$  channel complexes. *Nature* 599:158–164.

- Lee J, Moon S, Cha Y, Chung YD (2010) *Drosophila* TRPN (=NOMPC) channel localizes to the distal end of mechanosensory cilia. *PLoS One* 5:e11012.
- Li H, et al. (2022) Fly cell atlas: a single-nucleus transcriptomic atlas of the adult fruit fly. *Science* 375:eabk2432.
- Li B, Li S, Zheng H, Yan Z (2021) Nanchung and inactive define pore properties of the native auditory transduction channel in *Drosophila*. *Proc Natl Acad Sci U S A* 118:e2106459118.
- Metaxakis A, Oehler S, Klinakis A, Savakis C (2005) Minos as a genetic and genomic tool in *Drosophila melanogaster*. *Genetics* 171:571–581.
- Nadal MS, et al. (2003) The CD26-related dipeptidyl aminopeptidase-like protein DPPX is a critical component of neuronal A-type K<sup>+</sup> channels. *Neuron* 37:449–461.
- Nadrowski B, Albert JT, Göpfert MC (2008) Transducer-based force generation explains active process in *Drosophila* hearing. *Curr Biol* 18:1365–1372.
- Nagarkar-Jaiswal S, DeLuca SZ, Lee PT, Lin WW, Pan H, Zuo Z, Lv J, Spradling AC, Bellen HJ (2015) A genetic toolkit for tagging intronic MiMIC containing genes. *Elife* 4:08469.
- Oulé M, Atucha E, Wells TM, Macharadze T, Sauvage MM, Kreutz MR, Lopez-Rojas J (2021) Dendritic Kv4.2 potassium channels selectively mediate spatial pattern separation in the dentate gyrus. *iScience* 24:102876.
- Ping Y, Waro G, Licursi A, Smith S, Vo-Ba DA, Tsunoda S (2011) Shal/K<sub>v</sub>4 channels are required for maintaining excitability during repetitive firing and normal locomotion in *Drosophila*. *PLoS One* 6:e16043.
- Ravenscroft TA, Jacobs A, Gu M, Eberl DF, Bellen HJ (2023) The voltage-gated sodium channel in *Drosophila*, para, localizes to dendrites as well as axons in mechanosensitive chordotonal neurons. *eNeuro* 10:ENEURO.0105-23.2023.
- Riabinina O, Dai M, Duke T, Albert JT (2011) Active process mediates species-specific tuning of *Drosophila* ears. *Curr Biol* 21:658–664.
- Sheng M, Tsaur M-L, Jan YN, Jan LY (1992) Subcellular segregation of two A-type K<sup>+</sup> channel proteins in rat central neurons. *Neuron* 9:271–284.
- Thibault ST, et al. (2004) A complementary transposon tool kit for *Drosophila melanogaster* using *P* and *piggyBac*. *Nat Genet* 36:283–287.
- Tsunoda S, Salkoff L (1995) Genetic analysis of *Drosophila* neurons: *Shal*, *Shaw*, and *Shab* encode most embryonic potassium currents. *J Neurosci* 15:1741–1754.
- Venken KJT, et al. (2011) MiMIC: a highly versatile transposon insertion resource for engineering *Drosophila melanogaster* genes. *Nat Methods* 8:737–743.
- Walker RG, Willingham AT, Zuker CS (2000) A *Drosophila* mechanosensory transduction channel. *Science* 287:2229–2234.
- Wei A, Covarrubias M, Butler A, Baker K, Pak M, Salkoff L (1990) K<sup>+</sup> current diversity is produced by an extended gene family conserved in *Drosophila* and mouse. *Science* 248:599–603.
- Weinberger S, et al. (2017) Evolutionary changes in transcription factor coding sequence quantitatively alter sensory organ development and function. *Elife* 6:e26402.
- Yang S, Tang CM, Yang S (2015) The shaping of two distinct dendritic spikes by A-type voltage-gated K<sup>+</sup> channels. *Front Cell Neurosci* 9:469.